J|A|C|S
A R T I C L E S

Nanoporous Block Copolymer Micelle/Micelle Multilayer Films with Dual Optical Properties

Jinhan Cho,*,† Jinkee Hong,‡ Kookheon Char,*,‡ and Frank Caruso§

Contribution from the School of Advanced Materials Engineering, Kookmin University, Jeongneung-dong, Seongbuk-gu, Seoul 136-702, Korea, School of Chemical and Biological Engineering & NANO Systems Institute-National Core Research Center, Seoul National University, San 56-1, Shilim-dong, Kwanak-gu, Seoul 151-744, Korea, and Centre for Nanoscience and Nanotechnology, Department of Chemical and Biomolecular Engineering, The University of Melbourne, Victoria 3010, Australia

Received April 9, 2006; E-mail: khchar@plaza.snu.ac.kr; jinhan@kookmin.ac.kr

Abstract: We introduce a novel and versatile approach for preparing self-assembled nanoporous multilayered films with tunable optical properties. Protonated polystyrene-*block*-poly(4-vinylpyridine) (PS-*b*-P4VP) and anionic polystyrene-*block*-poly(acrylic acid) (PS-*b*-PAA) block copolymer micelles (BCM) were used as building blocks for the layer-by-layer assembly of BCM multilayer films. BCM film growth is governed by electrostatic and hydrogen-bonding interactions between the opposite BCMs. Both film porosity and film thickness are dependent upon the charge density of the micelles, with the porosity of the film controlled by the solution pH and the molecular weight (M_w) of the constituents. PS_{7K}-*b*-$P4VP_{28K}$/PS_{2K}-*b*-PAA_{8K} films prepared at pH 4 (for PS_{7K}-*b*-$P4VP_{28K}$) and pH 6 (for PS_{2K}-*b*-PAA_{8K}) are highly nanoporous and antireflective. In contrast, PS_{7K}-*b*-$P4VP_{28K}$/PS_{2K}-*b*-PAA_{8K} films assembled at pH 4/4 show a relatively dense surface morphology due to the decreased charge density of PS_{2K}-*b*-PAA_{8K}. Films formed from BCMs with increased PS block and decreased hydrophilic block (P4VP or PAA) size (e.g., PS_{36K}-*b*-$P4VP_{12K}$/PS_{16K}-*b*-PAA_{4K} at pH 4/4) were also nanoporous. This is attributed to a decrease in interdigitation between the adjacent corona shells of the low M_w BCMs, thus creating more void space between the micelles. Multilayer films with antireflective and photochromic properties were obtained by incorporating a water-insoluble photochromic dye (spiropyran) into the hydrophobic PS core of the BCMs assembled in the films. The optical properties of these films can be modulated by UV irradiation to selectively and reversibly control the transmission of light. Light transmission of higher than 99% was observed with accompanying photochromism in the (PS_{7K}-*b*-$P4VP_{28K}$/PS_{2K}-*b*-PAA_{8K}) multilayer films assembled at pH 4/6. Our approach highlights the potential to incorporate a range of materials, ranging from conventional hydrophilic materials with specific interactions to hydrophobic compounds, into the assembled BCMs to yield multifunctional nanoporous films.

Introduction

Nanoporous thin films have attracted considerable attention due to their potential application as antireflective films,[1−5] sensors,[6,7] membranes,[8−11] catalysts,[12,13] and electronic devices.[14,15] Efforts to prepare nanoporous films have mainly focused on post treatment methods, for example, solvent etching,[1] UV-,[2,16] thermal-,[17−20] acid-,[4,21−23] or salt-treatment.[24] Using this approach, porosity has been engineered into thin films

† Kookmin University.
‡ Seoul National University.
§ The University of Melbourne.
(1) Walheim, S.; Schaffer, E.; Mlynek, J.; Steiner, U. *Science* **1999**, *283*, 520−522.
(2) Ibn-Elhaj, M.; Schadt, M. *Nature* **2001**, *410*, 796−799.
(3) Hattori, H. *Adv. Mater.* **2001**, *13*, 51−54.
(4) Hiller, J.; Mendelsohn, J. D.; Rubner, M. F. *Nat. Mater.* **2002**, *1*, 59−63.
(5) Cebeci, F. C.; Wu, Z.; Zhai, L.; Cohen, R. E.; Rubner, M. F. *Langmuir* **2006**, *22*, 2856−2862.
(6) Chang, H.; Kosari, F.; Andreadakis, G.; Alam, M. A.; Vasmatzis, G.; Bashir, R. *Nano Lett.* **2004**, *4*, 1551−1556.
(7) Mara, A.; Siwy, Z.; Trautmann, C.; Wan, J.; Kamme, F. *Nano Lett.* **2004**, *4*, 497−501.
(8) Ding, Y.; Erlebacher, J. *J. Am. Chem. Soc.* **2003**, *125*, 7772−7773.
(9) Nair, B. N.; Suzuki, T.; Yoshino, Y.; Gopalakrishnan, S.; Sugawara, T.; Nakao, S.-I.; Taguchi, H. *Adv. Mater.* **2005**, *17*, 1136−1140.
(10) Shiflett, M. B.; Foley, H. C. *Science* **1999**, *17*, 1902−1905.
(11) Park, H. B.; Lee, Y. M. *Adv. Mater.* **2005**, *17*, 477−483.
(12) Gin, D. L.; Gu, W. *Adv. Mater.* **2001**, *13*, 1407−1410.
(13) Joo, S. H.; Choi, S. J.; Oh, I.; Kwak, J.; Liu, Z.; Terasaki, O.; Ryoo, R. *Nature* **2001**, *412*, 169−172.

(14) Kron, G.; Egerter, T.; Werner, J. H.; Rau, U. *J. Phys. Chem. B* **2003**, *107*, 3556−3564.
(15) Tian, Y.; Tatsuma, T. *J. Am. Chem. Soc.* **2005**, *127*, 7632−7637.
(16) Fu, G.-D.; Yuan, Z.; Kang, E.-T.; Neoh, K.-G.; Lai, D. M.; Huan, A. C. H. *Adv. Funct. Mater.* **2005**, *15*, 315−322.
(17) Kim, H.-C.; Wilds, J. B.; Kreller, C. R.; Volksen, W.; Brock, P. J.; Lee, V. Y.; Magbitang, T.; Hedrick, J. L.; Miller, R. D. *Adv. Mater.* **2002**, *14*, 1637−1639.
(18) Lee, B.; Park, Y.-H.; Hwang, Y.-T.; Oh, W.; Yoon, J.; Ree, M. *Nat. Mater.* **2005**, *4*, 147−150.
(19) Morgen, M.; Ryan, E. T.; Zhao, J.-H.; Hu, C.; Cho, T.; Ho, P. S. *Annu. Rev. Mater. Sci.* **2000**, *30*, 645−680.
(20) Huang, E.; Toney, M. F.; Volksen, W.; Mecerreyes, D.; Brock, P.; Kim, H.-C.; Hawker, C. J.; Hedrick, J. L.; Lee, V. Y.; Magbitang, T.; Miller, R. D. *Appl. Phys. Lett.* **2002**, *81*, 2232−2234.
(21) Zhai, L.; Nolte, A. J.; Cohen, R. E.; Rubner, M. F. *Macromolecules* **2004**, *37*, 6113−6123.
(22) Wang, Y.; Yu, A.; Caruso, F. *Angew. Chem., Int. Ed.* **2005**, *44*, 2888−2892.
(23) Cho, J.; Quinn, J. F.; Caruso, F. *J. Am. Chem. Soc.* **2004**, *126*, 2270−2271.
(24) Fery, A.; Scholer, B.; Cassagneau, T.; Caruso, F. *Langmuir* **2001**, *17*, 3779−3783.

of block copolymers, polymer blends, silicates, and multilayered films. Nanoporous films can also be prepared through the self-assembly of various building blocks, including charged silica particles[3,5,28] or artificially designed polymers.[29,30] In particular, these nanoporous films with low refractive indices (n_f) and film thicknesses in the range of about 80−160 nm, which is about one-quarter of the reference visible wavelength, can be applied as efficient antireflective coatings to improve the light transmission of transparent substrates in the visible wavelength range.[1−5] It is well known that glass or transparent plastic substrates with refractive indices of about 1.5 can display ideal antireflection with light transmission of almost 100% when a nanoporous film with a refractive index of about 1.22 is deposited on the substrate.

The layer-by-layer (LbL) assembly method offers diverse opportunities to prepare nanoporous thin films with multifunctional properties. An important advantage of this method is that it enables the preparation of films with tailored film thickness, composition, functionality on substrates of different size, and shape.[3,4,21−24,31−45] Additionally, various hydrophilic materials can be inserted within LbL films through complementary interactions (i.e., electrostatic,[1−5,24,28] hydrogen-bonding,[46,47] or covalent interaction[48]). Block copolymer micelles (BCMs) composed of hydrophilic and hydrophobic segments such as polystyrene-*b*-poly(acrylic acid) (PS-*b*-PAA) are known to incorporate hydrophobic materials (e.g., gold,[49,50] magnetic nanoparticles,[51] or fluorescent dyes[52]) into the hydrophobic core of micelles in water, and negatively charged PS-*b*-PAA containing hydrophobic dyes can be self-assembled with conventional polyelectrolytes (PEs) using the LbL method.[52] Therefore, our

motivation was to use BCMs in the fabrication of nanoporous thin films with integrated chemical, physical, and optical properties and tailored film nanostructure. A main aim was to modulate film nanostructure through the size of hydrophobic or hydrophilic BCM segments, as these influence the size and shape of the micelles formed in aqueous solution, including their solubility.[53]

In this study, we report the preparation of nanoporous BCM films, which are assembled making use of the electrostatic and hydrogen-bonding interactions between different BCMs, polystyrene-*block*-poly(4-vinylpyridine) (PS-*b*-P4VP) and anionic polystyrene-*block*-poly(acrylic acid) (PS-*b*-PAA). The charge densities and hence the adsorbed amount of the BCMs in the multilayer films were adjusted by varying the solution pH. Additionally, we demonstrate that the porosity of (PS-*b*-P4VP)/(PS-*b*-PAA) multilayer films can be controlled by varying either the charge density of the micelles or the hydrophobic (PS) and hydrophilic (P4VP or PAA) block sizes. We show that these films are highly efficient antireflective coatings, with more than 99% transmission observed from the BCMs with long hydrophilic corona chains and relatively high charge density. The nanoporous structure and antireflective properties of the films originate from the presence of two different kinds of BCMs in the multilayers; these properties are notably different from those observed for corresponding films containing one BCM, which are prepared by the alternate deposition with a polyelectrolyte (PE). For example, (PS-*b*-P4VP/PAA) or (P4VP/PS-*b*-PAA) have a relatively high refractive index ($n_f \approx 1.48$), and, as a result, these films do not significantly improve light transmission of transparent substrates such as glass ($n \approx 1.52$). The BCM nanoporous multilayer films were also used to incorporate the hydrophobic compound spiropyran into the PS cores, which allows optical switching of the films with respect to light transmission.

Experimental Section

Experimental details are given in the Supporting Information.

Results and Discussion

Formation of Nanoporous Structure. PS-*b*-P4VP block copolymers form cationic micelles with a hydrophobic PS core and a protonated P4VP shell in solutions at pH < 5. Above pH 5, PS-*b*-P4VP block copolymers are water-insoluble due to the deprotonation of P4VP segments.[52] PS-*b*-PAA forms anionic micelles due to the conversion from uncharged carboxylic acid groups (e.g., COOH) to charged carboxylic acid groups (e.g., COO$^-$) at pH > 3.[56] This phenomenon means that the charge densities of PS-*b*-P4VP and PS-*b*-PAA BCMs can be easily controlled by the solution pH as shown in Figure 1. The degree of ionization of PS-*b*-P4VP and PS-*b*-PAA was calculated on the basis of that of pure P4VP and PAA because the absorbance peaks of deprotonated pyridine (1600 cm^{-1}) and charged carboxylic acid groups (1570 cm^{-1}) are partially and fully overlapped with the aromatic ring of PS (see Supporting

(25) Prevo, B. G.; Hwang, Y.; Velev, O. D. *Chem. Mater.* **2005**, *17*, 3642−3651.
(26) Percec, V.; Dulcey, A. E.; Balagurusamy, V. S. K.; Miura, Y.; Smidrkal, J.; Peterca, M.; Nummelin, S.; Edlund, U.; Hudson, S. D.; Heiney, P. A.; Duan, H.; Magonov, S. N.; Vinogradov, S. A. *Nature* **2004**, *430*, 764−768.
(27) Reguera, J.; Fahmi, A.; Moriarty, P.; Girotti, A.; Rodriguez-Cabello, J. C. *J. Am. Chem. Soc.* **2004**, *126*, 13212−13213.
(28) Sun, L.; Chien, C.-L.; Searson, P. C. *Chem. Mater.* **2004**, *16*, 3125−3129.
(29) Sander, M. S.; Gao, H. *J. Am. Chem. Soc.* **2005**, *127*, 12158−12159.
(30) Oekermann, T.; Yoshida, T.; Minoura, H.; Wijayantha, K. G. U.; Peter, L. M. *J. Phys. Chem. B* **2004**, *108*, 8364−8370.
(31) Decher, G.; Hong, J.-D.; Schmitt, J. *Thin Solid Films* **1992**, *210*, 831−835.
(32) Decher, G. *Science* **1997**, *277*, 1232−1237.
(33) Caruso, F.; Caruso, R. A.; Möhwald, H. *Science* **1998**, *282*, 1111−1114.
(34) Shiratori, S. S.; Rubner, M. F. *Macromolecules* **2000**, *33*, 4213−4219.
(35) Mendelsohn, J. D.; Barrett, C. J.; Chan, V. V.; Pal, A. J.; Mayes, A. M.; Rubner, M. F. *Langmuir* **2000**, *16*, 5017−5023.
(36) Tang, Z.; Kotov, N. A.; Magonov, S.; Ozturk, B. *Nat. Mater.* **2003**, *2*, 413−418.
(37) Mamedov, A. A.; Kotov, N. A.; Prato, M.; Guldi, D. M.; Wicksted, J. P.; Hirsch, A. *Nat. Mater.* **2002**, *1*, 190−194.
(38) Wang, Y.; Caruso, F. *Chem. Mater.* **2005**, *17*, 953−961.
(39) Cho, J.; Char, K.; Hong, J.-D.; Lee, K.-B. *Adv. Mater.* **2001**, *13*, 1076−1078.
(40) Liang, Z.; Susha, A. S.; Caruso, F. *Adv. Mater.* **2002**, *14*, 1160−1164.
(41) Yu, A.; Liang, Z.; Cho, J.; Caruso, F. *Nano Lett.* **2003**, *3*, 1203−1207.
(42) Hua, F.; Shi, J.; Lvov, Y.; Cui, T. *Nano Lett.* **2002**, *2*, 1219−1222.
(43) Dubas, S. T.; Farhat, T. R.; Schlenoff, J. B. *J. Am. Chem. Soc.* **2001**, *123*, 5368−5369.
(44) Hammond, P. T. *Adv. Mater.* **2004**, *16*, 1271−1293.
(45) Jiang, C.; Markutsya, S.; Pikus, Y.; Tsukruk, V. V. *Nat. Mater.* **2004**, *3*, 721−728.
(46) Yang, S.; Zhang, Y.; Yuan, G.; Zhang, X.; Xu, J. *Macromolecules* **2004**, *37*, 10059−10062.
(47) Johnston, A. P. R.; Read, E. S.; Caruso, F. *Nano Lett.* **2005**, *5*, 953−956.
(48) Tian, Y.; He, Q.; Tao, C.; Li, J. *Langmuir* **2006**, *22*, 360−362.
(49) Kang, Y.; Taton, T. A. *Angew. Chem., Int. Ed.* **2005**, *44*, 409−412.
(50) Kang, Y.; Erickson, K. J.; Taton, T. A. *J. Am. Chem. Soc.* **2005**, *127*, 13800−13801.
(51) Kim, B.-S.; Qiu, J.-M.; Wang, J.-P.; Taton, T. A. *Nano Lett.* **2005**, *5*, 1987−1991.
(52) Ma, N.; Zhang, H.; Song, B.; Wang, Z.; Zhang, X. *Chem. Mater.* **2005**, *17*, 5065−5069.
(53) Terreau, O.; Luo, L.; Eisenberg, A. *Langmuir* **2003**, *19*, 5601−5607.
(54) Krevelen, D. W. V. *Properties of Polymers*; Elsevier: Amsterdam, The Netherlands, New York, 1990; Chapter 10.
(55) Bronstein, L. M.; Sidorov, S. N.; Zhirov, V.; Zhirov, D.; Kabachii, Y. A.; Kochev, S. Y.; Valetsky, P. M.; Stein, B.; Kiseleva, O. I.; Polyakov, S. N.; Shtykova, E. V.; Nikulina, E. V.; Svergun, D. I.; Khokhlov, A. R. *J. Phys. Chem. B* **2005**, *109*, 18786−18798.
(56) Choi, J.; Rubner, M. F. *Macromolecules* **2005**, *38*, 116−124.
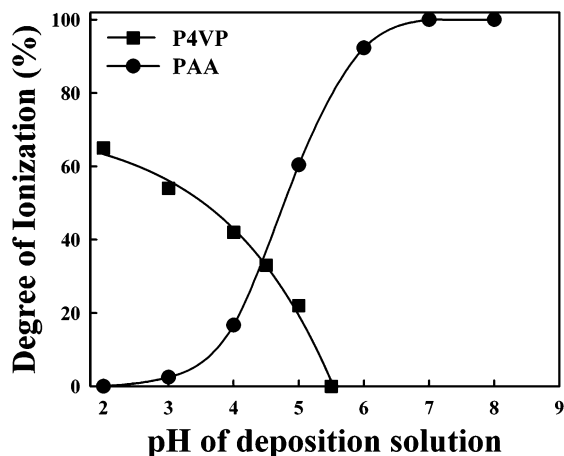
Figure 1. Change in the degree of ionization of P4VP and PAA as a function of pH. The FTIR absorbance spectra of P4VP and PAA were measured with increasing the solution pH from 2 to 5 and with decreasing the pH from 10 to 2, respectively.

Information, Figure S1). Additionally, the zeta-potentials of PS-*b*-P4VP and PS-*b*-PAA micelles were measured in aqueous solution (see Supporting Information, Experimental Section). The zeta-potentials of PS_{7K}-*b*-$P4VP_{28K}$, PS_{36K}-*b*-$P4VP_{12K}$, PS_{2K}-*b*-PAA_{8K}, and PS_{16K}-*b*-PAA_{4K} micelles at pH 4 were 24 ± 4.8, 23 ± 3.2, -26 ± 4.5, and -25 ± 3.7 mV, respectively. On the other hand, PS_{7K}-*b*-PAA_{28K} and PS_{16K}-*b*-PAA_{4K} micelles have the zeta potentials of -34 ± 3.2 and -33 ± 2.2 at pH 6, respectively. These results indicate that PS_{7K}-*b*-$P4VP_{28K}$ and PS_{36K}-*b*-$P4VP_{12K}$ micelles are positively charged at pH 4 and, on the other hand, PS_{2K}-*b*-PAA_{8K} and PS_{16K}-*b*-PAA_{4K} micelles are negatively charged at pH 4 and 6.

On the basis of the pH-sensitive characteristics of the formation of charged BCMs in aqueous solution, we measured the size of four different BCMs (PS_{7K}-*b*-$P4VP_{28K}$, PS_{36K}-*b*-$P4VP_{12K}$, PS_{2K}-*b*-PAA_{8K}, and PS_{16K}-*b*-PAA_{4K} micelles) adsorbed onto silicon substrates using tapping mode AFM (Figure 2). The charged micelles formed from PS_{7K}-*b*-$P4VP_{28K}$, PS_{36K}-*b*-$P4VP_{12K}$, PS_{2K}-*b*-PAA_{8K}, and PS_{16K}-*b*-PAA_{4K} deposited at pH 4 show micelle sizes of 9.8 ± 2.2 nm (Figure 2a), 14.2 ± 3.1 nm (Figure 2b), 7.2 ± 3.4 nm (Figure 2c), and 13.2 ± 2.6 nm, respectively. The PS_{7K}-*b*-PAA_{28K} and PS_{16K}-*b*-PAA_{4K} micelles formed at pH 6 have the sizes of 5.3 ± 1.2 nm (Figure 2e) and 12.0 ± 2 nm (Figure 2f), respectively. It is additionally shown that these micelles at pH 6 have relatively more uniform and regular size in comparison with those at pH 4 due to the increased electrostatic repulsion among negatively charged PAA blocks. These pH conditions used to form substrate-supported micelles, as depicted in Figure 1, were used to form BCM multilayer films.

UV−vis absorbance spectra of (PS_{7K}-*b*-$P4VP_{28K}$/PS_{2K}-*b*-PAA_{8K})$_n$ films prepared from the BCM solutions of pH 4/4 were investigated (see Supporting Information, Figure S2). The absorbance at 254 nm originates from the pyridine groups of PS_{7K}-*b*-$P4VP_{28K}$ micelles. The uniform growth of the absorbance peak at 254 nm (due to pyridine groups) indicates that the adsorbed amount of PS_{7K}-*b*-$P4VP_{28K}$ per bilayer is regular, demonstrating the BCM multilayer growth. The absorbance measured from 254 nm grows linearly with increasing bilayer numbers of PS_{7K}-*b*-$P4VP_{28K}$/PS_{2K}-*b*-PAA_{8K} (see Supporting Information, the inset of Figure S2).

We then investigated the adsorbed amount of PS-*b*-P4VP as a function of solution deposition pH for PS_{7K}-*b*-$P4VP_{28K}$ and PS_{2K}-*b*-PAA_{8K} (see Supporting Information, Figure S3). At pH 4, PS_{2K}-*b*-PAA_{8K} has about 18% of its carboxylic acid groups ionized, while about 42% of the pyridine groups in PS_{7K}-*b*-$P4VP_{28K}$ are protonated (see Figure 1). When the pH of PS_{7K}-*b*-$P4VP_{28K}$ solution is decreased to 3, PS_{7K}-*b*-$P4VP_{28K}$ is about 58% protonated, which induces the notable decrease in the number of PS_{7K}-*b*-$P4VP_{28K}$ micelles adsorbed. When the PS_{7K}-*b*-$P4VP_{28K}$ solution is held at pH 4 and the PS_{2K}-*b*-PAA_{8K} solution pH is increased from 4 (PS_{2K}-*b*-PAA_{8K} ∼18% ionized) to 6 (∼93% ionized), a decrease in the number of PS_{7K}-*b*-$P4VP_{28K}$ micelles adsorbed is also observed. The effect of solution pH on the BCM adsorbed amount is due to the electrostatic repulsion, originating from the increased charge density of protonated pyridine or anionic carboxylic acid groups. It is well known that for weak PEs such as poly(allylamine hydrochloride) (PAH) or poly(acrylic acid) (PAA), increasing the charge density yields the deposition of thinner layers due to stretched chain conformations.[23,34,56] Although the pH-dependent adsorption behavior originating from charged BCMs (i.e., P4VP blocks of PS_{7K}-*b*-$P4VP_{28K}$ or PAA blocks of PS_{2K}-*b*-PAA_{8K}) is similar to that of conventional weak PEs, the surface morphology obtained from the micelle/micelle multilayers is significantly different from that observed for PE multilayer films.

Figure 3 shows the influence of bilayer number (*n*) on the surface morphology of (PS_{7K}-*b*-$P4VP_{28K}$/PS_{2K}-*b*-PAA_{8K})$_n$ films deposited at pH 4/6. The small and largely spherical features (43 ± 2.1 nm diameter) seen in the (PS_{7K}-*b*-$P4VP_{28K}$/PS_{2K}-*b*-PAA_{8K})$_5$ film suggest that individual BCMs are involved in the multilayer to form such structure (Figure 3a), as the sizes of PS_{7K}-*b*-$P4VP_{28K}$ and PS_{2K}-*b*-PAA_{8K} measured from AFM are 9.8 ± 2.2 and 4.9 ± 0.8 nm, respectively (see Figure 2). The size of these features regularly increases with increasing the bilayer number. This is attributed to the BCMs selectively adsorbing to the oppositely charged preadsorbed micelle aggregates. The aggregate feature size for the 30-bilayer film is 110 ± 21 nm (see Figure 3e). Although the root-mean-square surface roughness of these films increases from 7 nm (5 bilayers) to about 30 nm (30 bilayers), due to the evolution of interconnected nanostructure, the film surfaces are highly uniform and homogeneous.

In this case, the film thickness, refractive index, and porosity[54] (see Supporting Information, Experimental Section) of the multilayer films, measured from ellipsometry, change from 42 nm, 1.19, and 55.2% for 10 bilayers to 104 nm, 1.25, and 42.8% for 30 bilayers (Figure 4 and Table 1). The porous structure of (PS_{7K}-*b*-$P4VP_{28K}$/PS_{2K}-*b*-PAA_{8K})$_n$ films deposited at pH 4/6 is formed through the hydrogen-bonding as well as the electrostatic interactions because partially protonated P4VP corona of PS_{7K}-*b*-$P4VP_{28K}$ are deprotonated in the PS_{2K}-*b*-PAA_{8K} solution of pH 6 (uncharged carboxylic acid groups ∼7%). However, we cannot exclude the possibility that the deposition of anionic PAA blocks onto the preadsorbed P4VP blocks can stabilize the protonated state of P4VP corona shells at pH 6. It has previously been reported that the degree of ionization of weak PEs
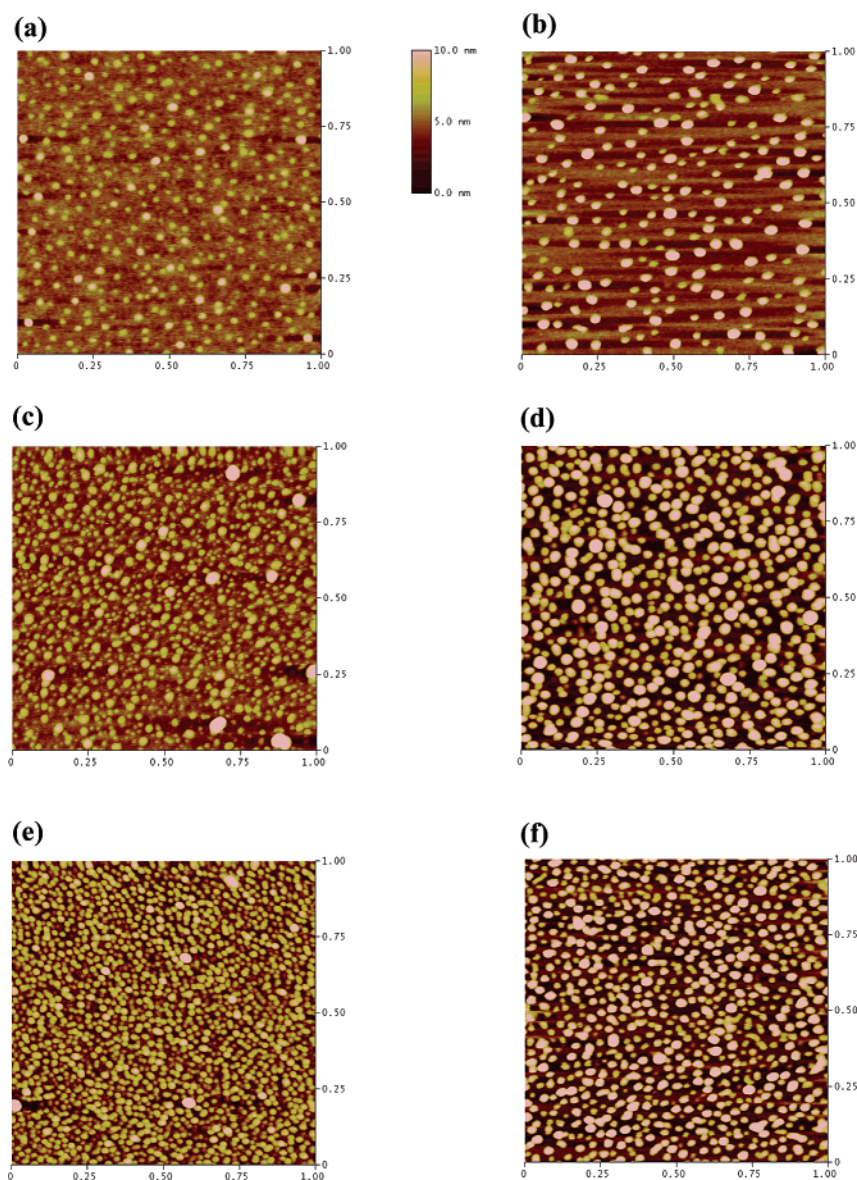
Figure 2. AFM images of (a) PS$_{7K}$-*b*-P4VP$_{28K}$, (b) PS$_{36K}$-*b*-P4VP$_{12K}$, (c) PS$_{2K}$-*b*-P4VP$_{8K}$, and (d) PS$_{16K}$-*b*-PAA$_{4K}$ micelles deposited onto Si wafers at pH 4 and AFM images of (e) PS$_{2K}$-*b*-PAA$_{8K}$ and (f) PS$_{16K}$-*b*-PAA$_{4K}$ micelles deposited at pH 6. The sizes of respective micelles measured from the height of AFM images are as follows: (a) 9.8 ± 2.2 nm, (b) 14.2 ± 3.1 nm, (c) 7.2 ± 3.4 nm, (d) 13.2 ± 2.6 nm, (e) 5.3 ± 1.2 nm, and (f) 12.0 ± 2.0 nm.

employed within the multilayers increases in comparison with that in bulk solution by deposition of oppositely charged PEs.[56,64−67]

Figure 5 schematically depicts the different stages during the formation of highly nanoporous multilayer films constructed from (PS$_{7K}$-*b*-P4VP$_{28K}$/PS$_{2K}$-*b*-PAA$_{8K}$) at pH 4/6. Initially, BCM micelles are adsorbed, with low surface coverage, on a substrate due to the electrostatic repulsion between like-charged species.

(57) Li, Q.; Quinn, J. F.; Caruso, F. *Adv. Mater.* **2005**, *17*, 2058−2062.
(58) Chabrera, I.; Krongauz, V. *Nature* **1987**, *326*, 582−585.
(59) Berkovic, G.; Krongauz, V.; Weiss, V. *Chem. Rev.* **2000**, *100*, 1741−1753.
(60) Zhu, L.; Khairutdinov, R. F.; Cape, J. L.; Hurst, J. K. *J. Am. Chem. Soc.* **2006**, *128*, 825−835.
(61) Zhao, W.; Carreira, E. M. *Org. Lett.* **2005**, *7*, 1609−1612.
(62) Evans, R. A. *Nat. Mater.* **2005**, *4*, 249−253.
(63) Yoo, D.; Shiratori, S. S.; Rubner, M. F. *Macromolecules* **1998**, *31*, 4309−4318.
(64) Xie, A. F.; Granick, S. *J. Am. Chem. Soc.* **2001**, *123*, 3175−3176.
(65) Xie, A. F.; Granick, S. *Macromolecules* **2002**, *35*, 1805−1813.
(66) Burke, S. E.; Barrett, C. J. *Langmuir* **2003**, *19*, 3297−3303.
(67) Kharlampieva, E.; Sukhishvili, S. A. *Langmuir* **2003**, *19*, 1235−1243.
(68) Petrov, A. I.; Antipov, A. A.; Sukhorukov, G. B. *Macromolecules* **2003**, *36*, 10079−10086.

This adsorption behavior is fully consistent with that observed from a variety of inorganic nanoparticles or PEs with high charge density.[63] During the next deposition step, the sparsely adsorbed micelles electrostatically associate with oppositely charged micelles, forming the high degree of interdigitation between relatively thick shells of PS$_{7K}$-*b*-P4VP$_{28K}$ and PS$_{2K}$-*b*-PAA$_{8K}$. These micelle structures are also confirmed in the phase image of AFM (Figure 5). With an increase in the bilayer deposition, the merged micelles increase in size and further deposition induces a highly nanoporous film structure.

We also investigated the SEM images of 5- and 8-bilayered PS$_{7K}$-*b*-P4VP$_{28K}$/PS$_{2K}$-*b*-PAA$_{8K}$ films deposited at pH 4/4 (see Supporting Information, Figure S4a and S4b). The 5-bilayer film is 32 nm thick (*d*), n_f = 1.18, and *P* (porosity) ≈ 57.4%, while the 8-bilayer film is 108 nm thick with n_f = 1.42 and *P* ≈ 12.5%. The low charge density (about 35% ionization of carboxylic acid groups) of PS$_{2K}$-*b*-PAA$_{8K}$ induces the formation of relatively large micellar aggregates due to the high degree

Figure 3. SEM images of nanoporous $(PS_{7K}\text{-}b\text{-}P4VP_{28K}/PS_{2K}\text{-}b\text{-}PAA_{8K})_n$ multilayer films formed at pH 4/6 as a function of bilayer number (n): (a) $n = 5$, (b) $n = 10$, (c) $n = 15$, (d) $n = 20$, and (e) $n = 30$.

of interdigitation between adjacent micelles. This yields a densely packed structure in the surface morphology with the increase on refractive index (see Supporting Information, Figure S4a and S4b) in comparison with those obtained at pH 4/6 (Figure 3a and 3e). In contrast, 3- and 7-bilayered ($PS_{36K}\text{-}b\text{-}P4VP_{12K}/PS_{16K}\text{-}b\text{-}PAA_{4K}$) films formed at pH 4/4 with a relatively high M_w hydrophobic PS segment and a low M_w hydrophilic segment form a highly interconnected nanostructure. The film properties are $d = 62$ nm, $n_f = 1.24$, and $P \approx 44.9\%$ for the 3-bilayered film (see Supporting Information, Figure S4c) and $d = 116$ nm, $n_f = 1.30$, $P \approx 33.2\%$ for the 7-bilayered film (see Supporting Information, Figure S4d). It is also noted that the corresponding small spherical micelles are more evident in the interconnected structure, unlike the ($PS_{7K}\text{-}b\text{-}P4VP_{28K}/PS_{2K}\text{-}b\text{-}PAA_{8K}$) films assembled at pH 4/4 or pH 4/6. This observation can be explained by the fact that the hydrophilic block chains (P4VP or PAA) of low M_w do not penetrate the shells of adjacent micelles to a larger extent, due to their relatively short chain length, yielding sparse vacancy between the neighboring micelles.
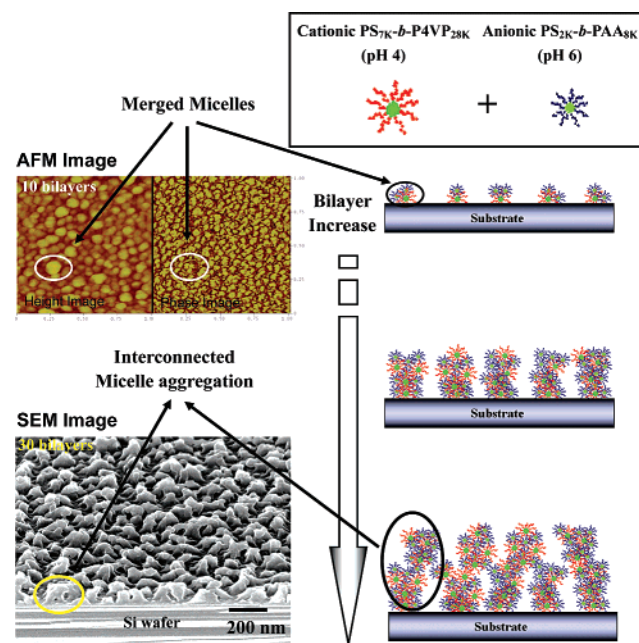
Antireflective Effect. On the basis of the highly nanoporous structure formed in the BCM/BCM multilayer films, we investigated the antireflective effect of these films. Figure 6a and b shows the light transmission of ($PS_{7K}\text{-}b\text{-}P4VP_{28K}/PS_{2K}\text{-}b\text{-}PAA_{8K}$)$_n$ multilayer films prepared with different solution pH combinations and block sizes. Film thickness was controlled in the range of $100-110$ nm for the maximum peak of light transmission in the visible wavelength of $500-600$ nm. For the ($PS_{7K}\text{-}b\text{-}P4VP_{28K}/PS_{2K}\text{-}b\text{-}PAA_{8K}$)$_n$ films shown in Figure 3e, the relatively high charge density of $PS_1\text{-}b\text{-}PAA_4$ (pH 6) results in the light transmission of 99.4% at 540 nm. However, the low charge density of $PS_{2K}\text{-}b\text{-}PAA_{8K}$ at pH 4 improves the light transmission only up to 96.5%. This decrease in light transmission is due to the decreased nanoporosity from the high degree of interdigitation between $PS_{7K}\text{-}b\text{-}P4VP_{28K}$ and $PS_{2K}\text{-}b\text{-}PAA_{8K}$ micelles or between slightly charged $PS_{2K}\text{-}b\text{-}PAA_{8K}$ micelles
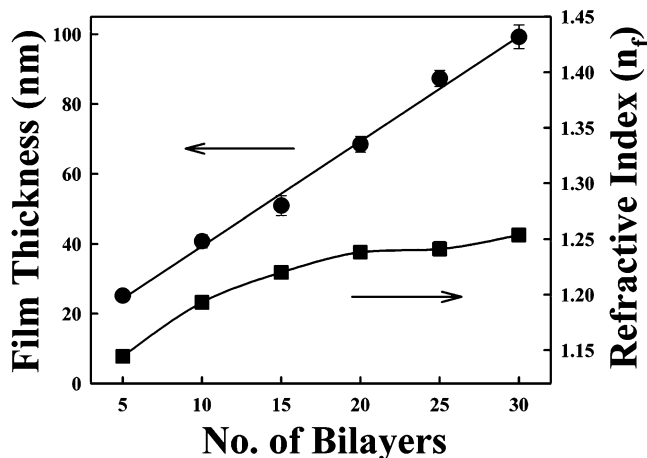
Figure 4. Change in film thickness and refractive index (n_f) of nanoporous (pH 4 PS$_{7K}$-*b*-P4VP$_{28K}$/pH 6 PS$_{2K}$-*b*-PAA$_{8K}$)$_n$ films with bilayer number (n) ranging from 5 to 30. Film thickness and refractive index were measured from ellipsometry.

Table 1. Change in the Total Thickness, Refractive Index, and Porosity of (PS$_{7K}$-*b*-P4VP$_{28K}$/PS$_{2K}$-*b*-PAA$_{8K}$)$_n$ pH 4/6 with Increasing Bilayer Number from $n = 5$ to 30

bilayer number (n)	total film thickness (nm)	refractive index (n_f)	porosity (%)
5	24.9	1.14	65.7
10	40.8	1.19	55.2
15	50.9	1.22	49.8
20	68.5	1.24	46.1
25	87.4	1.24	45.4
30	104.1	1.25	42.8

Figure 5. Schematic illustration of the self-assembly of nanoporous (PS$_{7K}$-*b*-P4VP$_{28K}$/PS$_{2K}$-*b*-PAA$_{8K}$)$_n$ multilayer films formed at pH 4/6 with the increase in bilayer number.

(see Supporting Information, Figure S4b). However, (PS$_{36K}$-*b*-P4VP$_{12K}$/PS$_{16K}$-*b*-PAA$_{4K}$)$_7$ films assembled at pH 4/4 with high M_w hydrophobic PS block and a low M_w hydrophilic P4VP (or PAA) demonstrate the light transmission above 99% at about 550 nm, despite the low charge density of PS$_{16K}$-*b*-PAA$_{4K}$. As
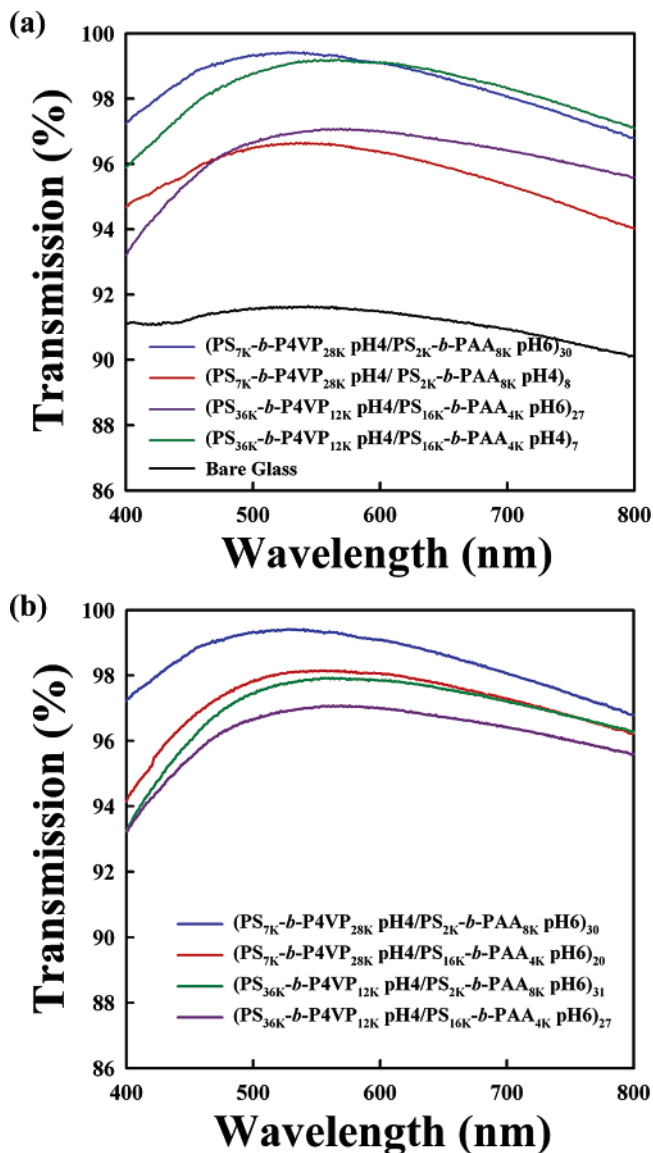
Figure 6. Light transmission curves of (a) (PS$_{7K}$-*b*-P4VP$_{28K}$/PS$_{2K}$-*b*-PAA$_{8K}$)$_n$ and (PS$_{36K}$-*b*-P4VP$_{12K}$/PS$_{16K}$-*b*-PAA$_{4K}$)$_n$ multilayer films assembled at different pH; (b) (PS-*b*-P4VP/PS-*b*-PAA)$_n$ films composed of different block size at pH 4/6.

mentioned earlier, this result is strongly supported by the formation of nanoporous structures (see Supporting Information, Figure S4d). That is to say, increasing the hydrophobic block segments effectively screens the degree of interdigitation between the hydrophilic corona chains of respective spherical micelles (i.e., same charged micelles or oppositely charged micelles) and results in the formation of voids. We also investigated the light transmission of (PS-*b*-P4VP/PS-*b*-PAA)$_n$ films prepared from the micelles carrying different block sizes at fixed pH's (pH 4/6). As shown in Figure 6b, the maximum light transmission of four different (PS-*b*-P4VP/PS-*b*-PAA)$_n$ films shows the range from 99.4% to 96.5%, demonstrating that the nanoporosity of these films can also be controlled by the block size as well as the solution pH. In particular, (PS$_{36K}$-*b*-P4VP$_{12K}$/PS$_{16K}$-*b*-PAA$_{4K}$)$_{27}$ films assembled at pH 4/6 show relatively low light transmission as compared to (PS$_{36K}$-*b*-P4VP$_{12K}$/PS$_{16K}$-*b*-PAA$_{4K}$)$_7$ films assembled at pH 4/4, despite the high charge density of PS$_{16K}$-*b*-PAA$_{4K}$ micelles. It is

considered that this observation is due to the formation of inhomogeneous surface morphology, possibly inducing the scattering of visible light (see Supporting Information, Figure S5). As a result, these data imply that the micelles (e.g., PS_{7K}-b-$P4VP_{28K}$ and PS_{2K}-b-PAA_{8K}) with small size, and relatively long and charged corona chains, lead to high light transmission in the BCM films. In addition, the difference in refractive index between the hydrophobic PS core ($n_f \approx 1.58$) and charged P4VP or PAA ($n_f \approx 1.47$) corona may also have an effect on the light transmission of PS-b-P4VP/PS-b-PAA multilayer films with different block sizes. Recently, Rubner and co-workers reported that the multilayer films composed of cationic poly(allyamine hydrochloride) and anionic silica nanoparticles ($n_f \approx 1.46$) of 7 nm in size show a relatively strong antireflective effect (light transmission above 99%) in comparison with that (98.8%) of a single layer film fabricated from 110 nm silica particles.[5]

Photochromic Effect. To demonstrate dual optical properties (i.e., photochromic property along with antireflective property) based on the BCM/BCM multilayer films, water-insoluble spiropyrans,[58−61] which have light-induced reversible isomerization between colorless spiropyran and colored forms of merocyanines,[61] were incorporated into the hydrophobic PS cores of PS_{7K}-b-$P4VP_{28K}$ (pH 4) and PS_{2K}-b-PAA_{8K} (pH 6) micelles to prepare photochromic nanoporous multilayer films. Up to date, most of the spiropyran derivatives, which have been extensively studied for applications in data memory and optical switching, have been embedded in sol−gel matrixes with organic solvent due to their low solubility in water. Our approach using micelles affords thickness-tunable thin films loaded with spiropyran. Based on this approach, the UV−vis absorption spectra of spiropyran-loaded $(PS_{7K}$-b-$P4VP_{28K}/PS_{2K}$-b-$PAA_{8K})_n$ films assembled at pH 4/6 were measured with increasing bilayer number ($n = 2−34$) (see Supporting Information, Figure S6). In this case, the absorbance spectra show distinct negative absorbance due to antireflection, with absorption peaks at 254 nm (for pyridine groups) and 367 nm (for spiropyran). Additionally, upon irradiation with 375 nm UV light for 15 min, the UV−vis absorption spectra for the $(PS_{7K}$-b-$P4VP_{28K}/PS_{2K}$-b-$PAA_{8K})_{34}$ film containing spiropyran show the decrease in the absorption peak at 367 nm (spiropyran form) and the growth of a new absorption peak at 550 nm (merocyanine form) (Figure 7a). The photocoloration of the spiropyran form under UV irradiation is caused by the C_{spiro}−O cleavage followed by the cis−trans isomerization leading to the merocyanine form. The new absorption peak at 550 nm slowly disappears when UV irradiation was stopped. This slow switching speed of photochromic dyes is presumably due to the rotational mobility of spiropyran molecules in the relatively rigid PS core. Evans et al. reported that the attachment of flexible oligomers with a low glass transition temperature (T_g) to photochromic dyes significantly increases the switching speed in a rigid polymer matrix.[62] Therefore, in view that hydrophobic block segments such as PS in the BCM micelles act as a nanocontainer for the incorporated hydrophobic compounds in aqueous media, the use of hydrophobic blocks with lower T_g in comparison with PS ($T_g \approx 100$ °C) or the use of photochromic dyes with flexible oligomers[59] can improve the switching speed of photochromic films.

When converting from these absorption spectra to light transmission curves, these films show the reversible photochro-
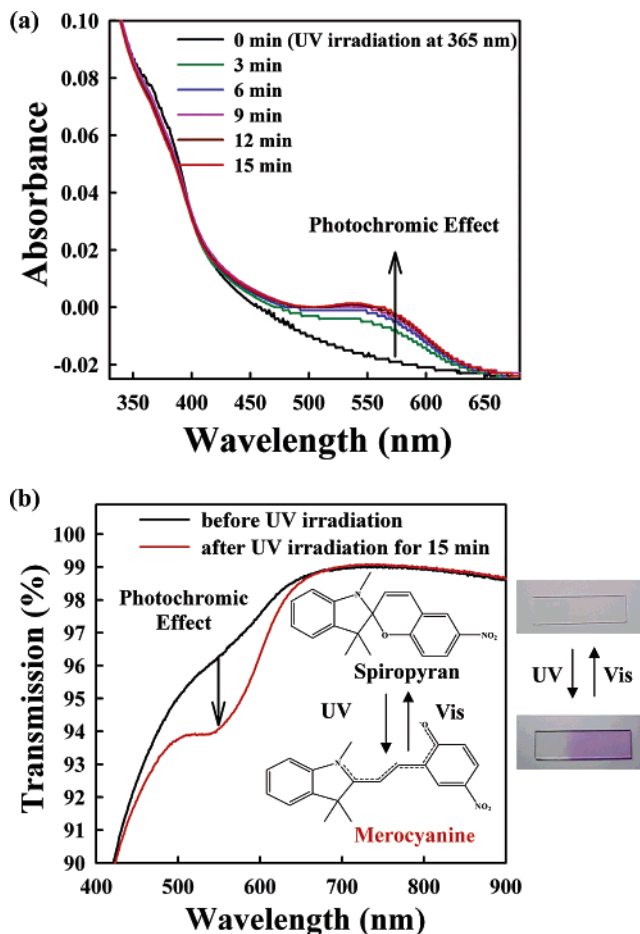
Figure 7. (a) Change in UV−vis spectra of spiropyran-loaded $(PS_{7K}$-b-$P4VP_{28K}/PS_{2K}$-b-$PAA_{8K})_{34}$ multilayer films with increasing UV irradiation time at 365 nm. (b) Light transmission curve of $(PS_{7K}$-b-$P4VP_{28K}/PS_{2K}$-b-$PAA_{8K})_{34}$ multilayer films before and after UV irradiation.

mic effect with about 99% light transmission between 650 and 900 nm (Figure 7b). These films showing both antireflective and photochromic effects selectively as well as reversibly improve the light transmission and filter the light at a desired wavelength by irradiating with UV light.

Conclusion

We have demonstrated the formation of highly nanoporous films composed of two different BCMs through layer-by-layer (LbL) assembly on substrates. The films thus prepared showed tunable optical properties, with strong antireflective properties with light transmission above 99%. The nanoporosity of these films can be controlled by the pH of deposition solution as well as the block size of BCM building blocks. The incorporation of water-insoluble spiropyran molecules into the PS cores of the BCMs in the multilayer films yields multifunctional nanoporous thin films with both antireflective and photochromic properties. These films with dual optical properties selectively and reversibly improve the light transmission and filter the desired wavelength of transmitted light, which can be controlled by the UV irradiation of the films. We regard our approach has a significant advantage in fabricating intelligent nanoporous films because various hydrophobic and/or hydrophilic materials can be physically and/or electrostatically confined within/onto BCMs and because nanoporosity can be induced without any

additional treatment. We are currently investigating BCM/BCM multilayer films containing two different kinds of hydrophobic nanoparticles within the hydrophobic cores of respective BCMs or hydrophilic (onto the charged corona shells of BCMs)/ hydrophobic inorganic nanoparticles (within the hydrophobic cores of BCMs). Considering the wide application areas of both LbL multilayers and block copolymer thin films, the approaches introduced in the present study are likely to open up new possibilities for devices with multifunctional properties.

Supporting Information Available: Details for experimental methods, FT-IR (Figure S1), UV−vis absorbance spectra (Figures S2, S3, and S6), and SEM images (Figures S4 and S5). This material is available free of charge via the Internet at http://pubs.acs.org.

JA062437Y